

# Improved potentials and Born-Oppenheimer corrections by new measurements of transitions of $^{129}\text{I}_2$ and $^{127}\text{I}^{129}\text{I}$ in the $\text{B}^3\Pi_{0_u^+} - \text{X}^1\Sigma_g^+$ band system<sup>\*</sup>

E.J. Salumbides<sup>1</sup>, K.S.E. Eikema<sup>1</sup>, W. Ubachs<sup>1</sup>, U. Hollenstein<sup>2</sup>, H. Knöckel<sup>3,a</sup>, and E. Tiemann<sup>3</sup>

<sup>1</sup> Laser Centre Vrije Universiteit, De Boelelaan 1081, 1081 HV Amsterdam, The Netherlands

<sup>2</sup> Laboratorium für Physikalische Chemie, ETH Zürich, 8093 Zürich, Switzerland

<sup>3</sup> Institut für Quantenoptik, Leibniz Universität Hannover, Welfengarten 1, 30167 Hannover, Germany

Received 26 October 2007 / Received in final form 7 February 2008

Published online 14 March 2008 – © EDP Sciences, Società Italiana di Fisica, Springer-Verlag 2008

**Abstract.** The light from one single frequency cw laser was employed in a double saturation spectroscopy experiment to record high resolution spectra of  $^{129}\text{I}_2$  and  $^{127}\text{I}^{129}\text{I}$  together with spectra of  $^{127}\text{I}_2$  which is used as a simultaneous frequency reference. Two separate saturation spectroscopy set ups were used. The frequencies of lines of  $^{129}\text{I}_2$  and  $^{127}\text{I}^{129}\text{I}$  were determined with respect to lines of  $^{127}\text{I}_2$ . More than 380 frequency differences between lines of  $^{127}\text{I}_2$  and of the other isotopomers have been included in the data set. By a direct potential fit a precise description of the potential energy curves of the B and the X state and of effective Born-Oppenheimer correction functions valid for all three isotopomers of  $\text{I}_2$  are given.

**PACS.** 33.15.Pw Fine and hyperfine structure – 33.20.-t Molecular spectra – 33.20.Kf Visible spectra

## 1 Introduction

The  $\text{B}^3\Pi_{0_u^+} - \text{X}^1\Sigma_g^+$  spectrum of the iodine molecule has long been employed as a frequency reference. The simplicity of just using a room temperature cell filled with iodine vapor for observation of spectra together with a proper laser source and the high density of lines in the spectrum led to many applications of laser stabilization to iodine absorption lines. Several of those lines are recommended as secondary frequency standards [1]. Additionally, systematic measurements of frequencies of iodine lines were performed by various laboratories, either in the form of spectral atlases [2,3] or in the form of tables of selected lines of vibrational bands (see e.g. [4–6]). Moreover, many measurements of selected iodine lines have been contributed by various authors. For a more complete list of papers before 2004 on measurements of iodine lines, see reference [7] and references therein. The precision of the transition frequencies is very high, a few lines have sub-MHz accuracy and more than 1500 have an accuracy in the range of a few MHz.

Thus this very precise data set is attractive for investigating small contributions to the molecular binding energies, like e.g. breakdown of the Born-Oppenheimer ap-

proximation, which is accounted for as additional terms in the Schrödinger equation [8].

The structure of the iodine B-X spectrum was modeled by Gerstenkorn and Luc [9] with a Dunham parameter approach based on the frequencies of the lines in their atlases. Extensive Fourier-transform laser induced fluorescence spectra were taken and modeled in Dunham based descriptions by Cerny et al. [10] for the three isotopomers  $^{127}\text{I}_2$ ,  $^{129}\text{I}_2$  and  $^{127}\text{I}^{129}\text{I}$ . However, the width of the lines was determined by the resolution of the Fourier-transform spectrometer, thus the precision was limited to a few times  $10^{-3} \text{ cm}^{-1}$ , and did not allow them to quantify effects of breakdown of the Born-Oppenheimer approximation.

High precision model descriptions of the  $\text{B}^3\Pi_{0_u^+} - \text{X}^1\Sigma_g^+$  spectrum have been proposed in previous papers [7,11,12], based on data of own investigations in the near infrared spectral region and on data from the literature. The task of accurately modeling the Doppler-free iodine spectrum has two distinct aspects. In addition to the electronic and rovibrational structure the iodine lines exhibit hyperfine structure. Models for the latter have been proposed [11] and were refined using new data of the other isotopomers in [12], yielding precise and concise formulas representing the dependence of the hyperfine parameters on the vibrational and rotational quantum numbers for  $^{127}\text{I}_2$ , which are valid for the other two isotopomers as well. For the rovibronic structure a global model description based on directly fitted potential energy curves was

<sup>\*</sup> Data set, parameters for the upper state potential, parameters for the ground state potential are available in electronic form at [www.epj.org](http://www.epj.org)

<sup>a</sup> e-mail: [knoeckel@iqo.uni-hannover.de](mailto:knoeckel@iqo.uni-hannover.de)

used in [7]. There it turned out that for a precise modeling of the transition frequencies, also Born-Oppenheimer correction (BOC) functions for adiabatic and nonadiabatic corrections had to be included in the Hamiltonian which determines the level energies involved in the optical transitions.

However, while the nonadiabatic centrifugal distortion correction (also called nonadiabatic BOC) can in principle be derived from one isotopomer alone, provided that data of a sufficiently large span of rotational lines are available, the adiabatic BOC can in principle only be determined when data of more than one isotopomer are included.

At the time when this model was developed, only six very precise transition frequencies from saturation spectroscopy for  $^{129}\text{I}_2$  and only one for  $^{127}\text{I}^{129}\text{I}$  existed in the literature [1]. Despite their high precision, this information about isotopic effects was not sufficient for a satisfactory determination of the complete BOC. Thus it was not clear at the end of [7], how reliable the BOC functions would be, especially because a comparison of the expectation values of the nonadiabatic BOC calculated with the vibrational eigenfunctions did not agree well with the experimentally determined  $g_J$  factors (see Sect. 4 of [7]).

With the very precise data on the iodine B-X system we have in principle a data set with which one can investigate how precisely the BOC parameters can be evaluated for such a heavy system. However, to that end more data of high accuracy from other isotopomers are necessary. Therefore, a joint effort between VU Amsterdam and Leibniz University of Hannover undertook to measure a substantial amount of transition frequencies for the homonuclear isotopomer  $^{129}\text{I}_2$  and the mixed one  $^{127}\text{I}^{129}\text{I}$ . Here we report on the rovibronic transition frequencies of these measurements. In Section 2 we describe the experimental procedure applied. In Section 3 details of the measurements and in Section 4 details of the evaluation procedure are presented. In Section 5 we discuss the model fit and its results. A conclusion will summarize the “take home message” of the paper.

## 2 Experimental

A schematic layout of the experimental setup is shown in Figure 1. A stabilized, tunable cw ring-dye-laser (Spectra Physics 380D) is used as the common radiation source. The dye laser is operated with Rhodamine 6G dye to access the wavelength range from 573 nm to 583 nm, while Rhodamine B dye is used for the range 610 nm to 615 nm and for some measurements near 633 nm.

Two distinct saturated absorption setups allow for the simultaneous recording of the spectra obtained from a vapor cell containing the isotopomers  $^{129}\text{I}_2$  and  $^{127}\text{I}^{129}\text{I}$  together with that of the main isotopomer  $^{127}\text{I}_2$  in another cell. By means of this double saturation setup, the spectra of the isotopomers  $^{129}\text{I}_2$  and  $^{127}\text{I}^{129}\text{I}$  can be referred to the  $^{127}\text{I}_2$  resonances that have been measured at high accuracy before [4,5]. With reference to this spectrum, the data on the  $^{129}\text{I}$  containing species can be calibrated on a relative scale and on an absolute scale as well.

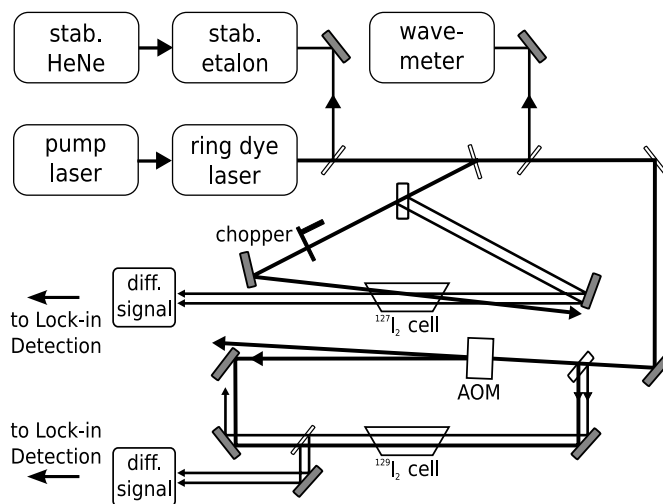


**Fig. 1.** Scheme of the experimental setup. It consists of two parallel saturation spectroscopy measurements on two distinct vapor cells. One cell contains about 85% of  $^{129}\text{I}$  and about 15% of  $^{127}\text{I}$ , giving rise to spectra of  $^{129}\text{I}_2$  (and  $^{127}\text{I}^{129}\text{I}$  and weak  $^{127}\text{I}_2$ ). The other cell contains pure  $^{127}\text{I}_2$ . The positions of the  $^{129}\text{I}_2$  and  $^{127}\text{I}^{129}\text{I}$  resonances are determined with respect to the position of  $^{127}\text{I}_2$  lines by means of a HeNe-stabilized étalon used as a ruler.

A 10-cm vapor cell containing 100%  $^{127}\text{I}_2$  is used in one of the saturation setups, identical to the one used in the previous studies discussed in references [4,5]. Differential absorption by two probe beams is monitored, while one of them is crossed at a slight angle ( $<7$  mrad) with the saturating beam, leading to a contribution to the Doppler width of about 2.5 MHz. The saturating beam is modulated by a mechanical chopper at around 700 Hz and lock-in signal detection is employed. The  $^{127}\text{I}_2$  cell is used at room temperature, corresponding to a vapor pressure of about 27 Pa [13].

A 5-cm cell containing mainly  $^{129}\text{I}$  and a small amount of  $^{127}\text{I}$  is used in the other saturation setup. The pump-offset saturation spectroscopy technique [14,15] is applied to maximize the signal detection sensitivity. The first-order diffraction beam from an acousto-optic modulator (AOM) shifted by +75 MHz is used as the saturating beam. As a consequence of the 75-MHz frequency offset of the saturating beam with respect to the probe beams, the saturation resonances are shifted by 37.5 MHz from the real line positions [14,15] to lower frequencies of the laser. Differential absorption signals were acquired, with one of the probe beams overlapped collinearly with the saturating beam. A 50-kHz modulation was imposed on the amplitude of the saturating beam and the saturation signal is retrieved by lock-in detection. The inherent sensitivity of the pump-offset technique combined with the fast modulation of the AOM results in a high detection sensitivity. With such a scheme, we could also detect the strong transitions of the  $^{127}\text{I}_2$  molecules that are present, but only in trace amounts, inside this cell. These weak  $^{127}\text{I}_2$  signals are compared to those obtained from the parallel  $^{127}\text{I}_2$

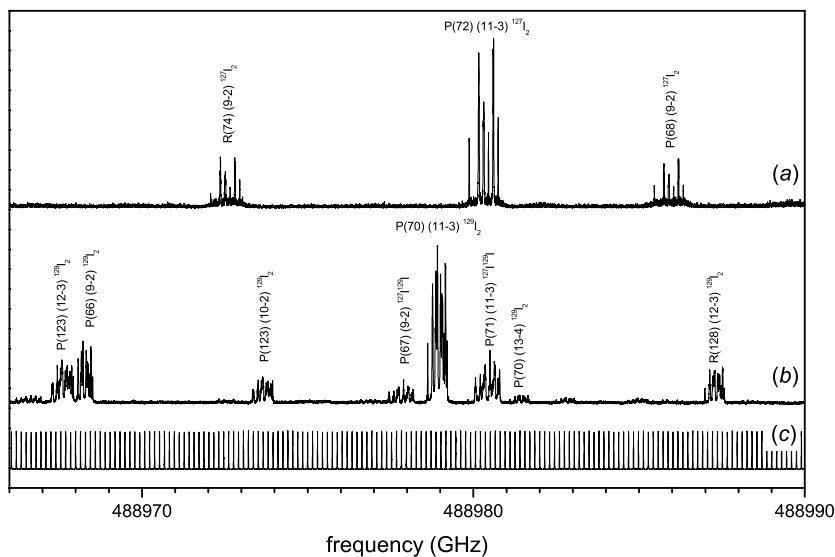


**Fig. 2.** Typical spectra recorded while tuning the laser frequency. Trace (a) corresponds to the setup with a cell containing natural iodine, which is composed of 100% of  $^{127}\text{I}$ . Trace (b) corresponds to the  $^{129}\text{I}_2$  cell. With its content of few % of  $^{127}\text{I}$  also lines of  $^{127}\text{I}^{129}\text{I}$  appear, and moreover, weak lines of  $^{127}\text{I}_2$ . The lines of trace (b) are shifted by 37.5 MHz to lower frequencies due to the AOM frequency of 75 MHz. The lower trace (c) shows marker peaks from the stabilized étalon, which is used for interpolation of frequency differences.

saturation setup in order to check for possible frequency shifts between the two saturation setups.

A wave meter is used to coarsely tune the laser to the resonances. Difference frequency measurements are carried out by employing the transmission peaks of a calibrated 50-cm Fabry-Perot étalon. The étalon temperature and pressure is stabilized and its length is actively locked to the wavelength of a Zeeman-stabilized He-Ne laser. The étalon free spectral range FSR is measured at the start of every measurement session, and has a typical value of 148.96(1) MHz with small day-to-day variations. For the absolute frequency calibration of the  $^{129}\text{I}_2$  and  $^{127}\text{I}^{129}\text{I}$  lines a nearby  $^{127}\text{I}_2$  line was chosen as reference which had been measured previously in references [4,5]. Since the largest separation was less than thirty étalon fringes, this procedure results in a 1 MHz uncertainty of frequency differences.

### 3 Measurements

With the goal to cover as many rovibronic bands as possible in the ranges available by the tuning range of the dye laser we observed simultaneously saturated absorption spectra from both setups. In different periods of measurements around 633 nm, from 615 to 610 nm, and from 583 to 573 nm were chosen. The hyperfine structures of lines of rovibronic bands for  $v''$  ranging from 0 to 5, for  $v'$  ranging from 9 to 20, and  $J''$  ranging from 23 to 128 were recorded for all three isotopomers. An example of such recorded spectra is given in Figure 2. The upper trace (a) shows the saturation spectrum from the frequency reference setup with the  $^{127}\text{I}_2$  cell. The middle trace (b) shows that for the  $^{129}\text{I}$  cell. In the lowest trace the frequency markers from the reference cavity are shown. The individual frequency sweeps were selected such that in each scan at least one hyperfine component with an absolute frequency already known from [4,5] was located.

Thus an absolute frequency calibration of the recorded spectra is easily possible. A relative frequency scale was established from the markers of the Fabry-Pérot cavity applying a spline fit and a linearisation procedure to the series of markers. After that this relative scale was converted to an absolute one by linking it to one of the hyperfine components known with high accuracy. For the record of Figure 2 e.g., the lowest frequency hyperfine component  $a_1$  (sometimes also called ‘ $t$ ’ component) of the line P(72) (11-3) served as the calibration line for the absolute frequency.

For obtaining the pure rovibronic transition frequencies, first the hyperfine structure was fitted and the hyperfine-free transition frequency determined from the fit. The details of the hyperfine structure models have been discussed in [12] and will not be repeated here. For more information about the hyperfine structure fits of the different isotopomers, taking into account a residual Doppler background and absorption in the case of the longer  $^{127}\text{I}_2$  cell, the reader is referred to that paper.

From such evaluation on a relative frequency scale the absolute calibration of the frequencies of the lines of all isotopomers is possible. However, frequency differences between lines are more precise because only the uncertainty coming from the calibration of the stabilized reference cavity has to be taken into account, while for an absolute calibration the uncertainty of the reference line also must be accounted for. Therefore, in most cases we determined difference frequencies of  $^{129}\text{I}_2$  and  $^{127}\text{I}^{129}\text{I}$  with respect to chosen lines of  $^{127}\text{I}_2$  from the other setup. Such differences were corrected for the systematic shift of 37.5 MHz of the spectra from the different setups due to the use of the AOM. In order to detect other possible systematic shifts between the different setups, we verified this procedure for the shifts of lines of the main isotopomer  $^{127}\text{I}_2$  in cases where its lines could be identified in spectra recorded in the setup for the other isotopomers. The typical uncertainty of the absolute calibration by  $^{127}\text{I}_2$  lines

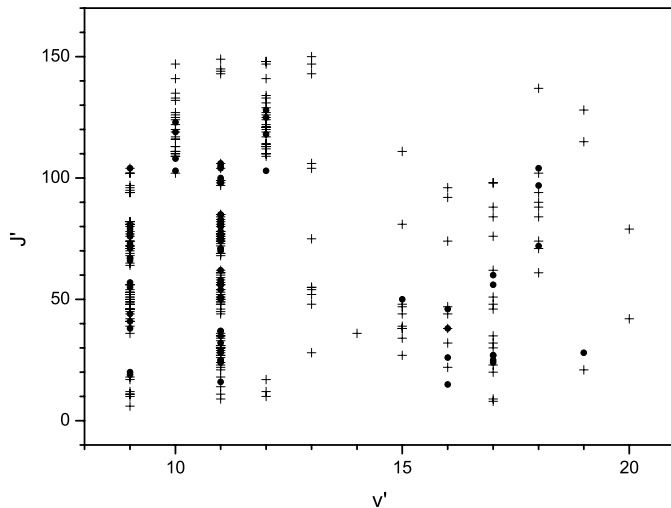


**Fig. 3.** Data field in terms of the upper vibrational and rotational quantum numbers of the transitions of the isotopomers of  $I_2$ . Crosses mark the data of  $^{129}I_2$ , while dots mark data of the mixed isotopomer  $^{127}I^{129}I$ . The vibrational quantum numbers of the ground state levels range from  $v'' = 0$  to  $v'' = 5$ .

is 1 MHz ( $1\sigma$ ). The residual uncertainty of the frequency differences is mainly determined by some uncorrected nonlinearities or non-uniformity of the laser scan between two markers, which cannot be detected due to the marker separation and which is left after the computerized linearisation procedure; it is assumed to be not larger than 1.5 MHz.

Altogether more than 290 difference frequencies for  $^{129}I_2$  and more than 90 difference frequencies for  $^{127}I^{129}I$  were acquired. An overview of the quantum number range in the upper state is shown in Figure 3. The crosses mark data for the homonuclear isotopomer  $^{129}I_2$ , while the dots give the data field for the mixed  $^{127}I^{129}I$ . Vibrational quantum numbers for the lower state range from  $v'' = 0$  to  $v'' = 5$ . The data for the main isotopomer  $^{127}I_2$  span the range of vibrational quantum numbers  $0 \leq v' \leq 43$  for the upper and  $0 \leq v'' \leq 17$  for the lower state.

## 4 Modeling of the spectra

The observed spectra will be modeled as in our recent paper [7], with the physical approach of describing each electronic state directly by a potential, and the energies of the levels being determined as the eigenvalues of the Schrödinger equation solved with these potentials. The potentials are represented in a parametrized form involving parameters which are fitted. We will model the case of single state (Born-Oppenheimer) potentials, allowing only for the lowest order corrections of the Born-Oppenheimer approximation. The data range is selected such that local perturbations by other electronic states, which are known to occur close to the dissociation limits [16–18] of the ground or excited state, are kept outside the selected energy ranges. For the levels of the B state which are in

the region of known predissociation caused by the repulsive  $^1II_u$  state crossing the B state [19–21], we neglect any local effect of level shifts. The levels in the data set are from high resolution experimental observations and the observed spectra showing narrow lines and regular intensities in the hyperfine patterns certify that the degree of predissociation should be small enough that such shifts will be absorbed in the present single state model within the presently obtainable precision.

Several representations of the potentials in such direct potential fits have been proposed in the literature, like e.g. the expanded Morse oscillator [22] or modified Lennard-Jones potential [23]. These were developed to describe the whole potential from short to large internuclear separations in a single expression which can be designed so that also the asymptotic behavior at large internuclear distance is described correctly (see e.g. [24]). Other approaches like the spline interpolated numerical potential by Pashov et al. [25] use a flexible spline based representation for the range of intermediate nuclear distances for which data are available, and apply smoothly analytical extensions for the short and long range parts which are not supported by data.

We will follow here our previous approach in [7] and use potentials in the so-called “X-representation”. The potential is composed of three sections. The central well, which will determine the energy eigenvalues of the observed levels, is written as a truncated power series of the form

$$V(R) = \sum_i a_i X^i, \quad i = 0, 1, 2, \dots \quad (1)$$

with

$$X = \frac{R - R_m}{R + bR_m}. \quad (2)$$

The parameters  $a_i$  are adjusted in a fit,  $R$  is the internuclear distance and  $R_m$  is an arbitrarily chosen expansion center close to the equilibrium nuclear distance of the electronic state. The parameter  $b$  allows us to vary the nonlinear mapping function  $X(R)$ , and is adjusted only once for a best fit of the potential representation (1) to the potential to start with.

Sufficiently far out of the range of internuclear distances in which the potential is determined by experimental data, the intermediate potential is continued to smaller and to larger internuclear distances by physically appropriate extension functions. For the inner branch  $R < R_I$ ,  $R_I$  being the joining abscissa with the intermediate part, an exponential

$$V(R) = A_I \exp(-B_I(R - R_I)) \quad (3)$$

is used. The parameters  $A_I$  and  $B_I$  are adjusted to give a smooth and differentiable connection at  $R_I$  after each modification of the central part of the potential. The outer branch at  $R > R_O$ ,  $R_O$  being the joining point with the intermediate part, is extended with functions representing dispersion interactions

$$V(R) = D_e - \sum_n \frac{C_n}{R^n} - A_O \exp(-B_O(R - R_O)). \quad (4)$$

**Table 1.** Potential data of the upper state B<sup>3</sup>Π<sub>0<sub>u</sub><sup>+</sup> and lower state X<sup>1</sup>Σ<sub>g</sub><sup>+</sup> and of the BOC functions α(R) and V<sub>ad</sub>(R) for the reference isotopomer <sup>127</sup>I<sub>2</sub>.</sub>

Parameter	Upper state B0 <sub>u</sub> <sup>+</sup>	Lower state X <sup>1</sup> Σ <sub>g</sub> <sup>+</sup>
R <sub>m</sub> [Å]	3.02669183	2.66638233
b	-0.75	-0.60
a <sub>0</sub> [cm <sup>-1</sup> ]	15769.067837	0.0
a <sub>1</sub> [cm <sup>-1</sup> ]	0.813930E+01	0.155389E+00
a <sub>2</sub> [cm <sup>-1</sup> ]	0.850290979E+04	0.492601477E+05
a <sub>3</sub> [cm <sup>-1</sup> ]	0.695677594E+04	0.213629963E+05
a <sub>4</sub> [cm <sup>-1</sup> ]	0.995264129E+03	-0.18173865E+05
a <sub>5</sub> [cm <sup>-1</sup> ]	-0.556338644E+04	-0.49468474E+05
a <sub>6</sub> [cm <sup>-1</sup> ]	-0.1074389661E+05	-0.71353991E+05
a <sub>7</sub> [cm <sup>-1</sup> ]	-0.1685419562E+05	-0.10110925E+06
a <sub>8</sub> [cm <sup>-1</sup> ]	-0.1533164369E+05	-0.7156108E+05
a <sub>9</sub> [cm <sup>-1</sup> ]	0.4315045697E+05	0.4710538E+06
a <sub>10</sub> [cm <sup>-1</sup> ]	0.6251096110E+05	-0.2904654E+06
a <sub>11</sub> [cm <sup>-1</sup> ]	-0.38914630400E+06	-0.73300648E+07
a <sub>12</sub> [cm <sup>-1</sup> ]	-0.43219553147E+06	0.22578115E+07
a <sub>13</sub> [cm <sup>-1</sup> ]	0.27235279905E+07	0.38250822E+08
a <sub>14</sub> [cm <sup>-1</sup> ]	0.32186808611E+07	
a <sub>15</sub> [cm <sup>-1</sup> ]	-0.127338590547E+08	
a <sub>16</sub> [cm <sup>-1</sup> ]	-0.172752514874E+08	
a <sub>17</sub> [cm <sup>-1</sup> ]	0.425255265406E+08	
a <sub>18</sub> [cm <sup>-1</sup> ]	0.712695731657E+08	
a <sub>19</sub> [cm <sup>-1</sup> ]	-0.9130578539938E+08	
a <sub>20</sub> [cm <sup>-1</sup> ]	-0.2108682403457E+09	
a <sub>21</sub> [cm <sup>-1</sup> ]	0.9267186544061E+08	
a <sub>22</sub> [cm <sup>-1</sup> ]	0.4132330557779E+09	
a <sub>23</sub> [cm <sup>-1</sup> ]	0.6085337864116E+08	
a <sub>24</sub> [cm <sup>-1</sup> ]	-0.4879703383624E+09	
a <sub>25</sub> [cm <sup>-1</sup> ]	-0.3052394100029E+09	
a <sub>26</sub> [cm <sup>-1</sup> ]	0.2691855865112E+09	
a <sub>27</sub> [cm <sup>-1</sup> ]	0.3494609136897E+09	
a <sub>28</sub> [cm <sup>-1</sup> ]	0.2771015696362E+08	
a <sub>29</sub> [cm <sup>-1</sup> ]	-0.1333716748717E+09	
a <sub>30</sub> [cm <sup>-1</sup> ]	-0.7655507971445E+08	
a <sub>31</sub> [cm <sup>-1</sup> ]	-0.1366495310913E+08	
α <sub>0</sub>	-0.23586E-03	*
α <sub>1</sub>	0.23445E-04	*
α <sub>2</sub>	-0.43703E-03	*
α <sub>3</sub>	-0.39630E-03	*
α <sub>4</sub>	-0.10191E-02	*
α <sub>5</sub>	-0.16462E-03	*
v <sub>0</sub> [cm <sup>-1</sup> ]	-0.209726E+00	*
v <sub>1</sub> [cm <sup>-1</sup> ]	-0.668183E+01	*
v <sub>2</sub> [cm <sup>-1</sup> ]	0.154676E+01	*
v <sub>3</sub> [cm <sup>-1</sup> ]	-0.286898E+01	*
l	5	
Extension data used		
R <sub>I</sub> [Å]	2.64700	2.40000
A <sub>I</sub> [cm <sup>-1</sup> ]	0.19605269E+05	0.45809329E+04
B <sub>I</sub> [Å <sup>-1</sup> ]	0.13736027E+01	0.90168320E+01
R <sub>O</sub> [Å]	4.90000	3.30000
A <sub>O</sub> [cm <sup>-1</sup> ]	-0.8105289769E+01	0.1053614048E+04
B <sub>O</sub> [Å <sup>-1</sup> ]	0.9347221716E+01	0.1259030368E+01
D <sub>e</sub> [cm <sup>-1</sup> ]	20150.317 [27]	12547.340 [27]
C <sub>5</sub> [cm <sup>-1</sup> Å <sup>5</sup> ]	0.3161E+06 [28]	-
C <sub>6</sub> [cm <sup>-1</sup> Å <sup>6</sup> ]	0.1506E+07 [28]	0.148E+07 [26]
C <sub>8</sub> [cm <sup>-1</sup> Å <sup>8</sup> ]	0.2480E+08 [28]	0.386E+08 [26]
C <sub>10</sub> [cm <sup>-1</sup> Å <sup>10</sup> ]	0.4200E+09 [28]	0.10E+09 [26]
Range of turning points of data set [Å]	2.650–4.589	2.427–3.079
R <sub>e</sub> ( <sup>127</sup> I <sub>2</sub> ) [Å]	3.0264	2.6664
T <sub>e</sub> ( <sup>127</sup> I <sub>2</sub> ) [cm <sup>-1</sup> ]	15769.0659	0.0000

\* no parameter included in fit, see text.

The parameters  $D_e$  and  $C_n$  are taken from literature [26–28], and the same values are taken for all isotopomers. This is justified because this part of the long range extension is far enough from the levels determined by the data that small changes like the atomic isotope shift do not introduce significant changes of the eigenvalues in the central part  $R_I \leq R \leq R_O$  of the potential within the present accuracy. The numerical values so determined are given in Table 1. The exponential term is used to insure smoothness and differentiability at the connection  $R_O$ , and its parameters are adjusted accordingly after each modification of the central part of the potential. Thus, it does not have a physical meaning of an exchange term.

Small energy contributions which are neglected within the Born-Oppenheimer approximation (“Born-Oppenheimer corrections”, BOC) are considered because of the very accurate data. A complete set of BOC would include an adiabatic correction  $V_{corr}$  of the potential, a nonadiabatic correction term  $\alpha(R)$  in the rotational Hamiltonian and a nonadiabatic contribution  $\beta(R)$  to the kinetic energy operator. For a homonuclear molecule these corrections depend on the ratio  $\frac{m_e}{\mu}$  of the electron mass  $m_e$  and the reduced mass  $\mu$  of the molecule. Watson [8,29] showed, that only two of these corrections can be determined simultaneously. Moreover, due to the mass dependence the contributions by  $\beta$  are expected to be very small [30]. Thus we chose  $\beta = 0$  in our approach; contributions of it will be absorbed in effective BOC functions  $V_{corr}(R)$  and  $\alpha(R)$ , and the effective Hamiltonian for the radial motion is written as [7,29,30]:

$$\mathbf{H}_{eff} = -\frac{\hbar^2}{2\mu} \frac{\partial^2}{\partial R^2} + V(R) + V_{corr}(R) + \frac{\hbar^2[1 + \alpha(R)]J(J+1)}{2\mu R^2}. \quad (5)$$

For both  $V_{corr}$  and  $\alpha$  we employ functions of the internuclear distance  $R$  represented as a truncated power series in  $X$ :

$$\alpha(R) = \frac{\mu_{ref}}{\mu} V_{nad} \quad (6)$$

with

$$V_{nad} = \frac{2R_m}{R + R_m} \sum_i \alpha_i X^i, i = 0, 1, 2, \dots \quad (7)$$

and

$$V_{corr}(R) = \left(1 - \frac{\mu_{ref}}{\mu}\right) V_{ad} \quad (8)$$

with

$$V_{ad} = \left(\frac{2R_m}{R + R_m}\right)^l \sum_i v_i X^i, i = 0, 1, 2, \dots \quad (9)$$

with  $\mu_{ref}$  being the reduced mass of the selected reference isotope  $^{127}\text{I}_2$  and  $l$  being the power of  $R$  in the leading term of the dispersion interaction of equation (4). The adiabatic correction  $V_{corr}(R)$  can only be determined if data of different isotopic species of the molecule are included. This ansatz should consider the asymptotic behaviour of

the correction  $V_{corr} = V_{corr}(B) - V_{corr}(X)$  such that it asymptotically corresponds to the atomic isotope shift [31] of the  $^2\text{P}_{1/2} - ^2\text{P}_{3/2}$  transition of iodine. However, to our knowledge this isotope shift is not yet known experimentally, but it is expected to be small because the transition is only due to a change in the fine structure level. Thus here we force the asymptotic value of  $V_{corr}$  to zero at infinity. The influence of this choice on the eigenvalues is negligibly small as the energies of the highest levels described with the model are still far from the dissociation energy. For the adiabatic and the nonadiabatic corrections the representations of equations (7)–(9) were used for the full range of  $R$  without any extensions such as those for the potential function model.

During the fit the eigenvalues for the lower and the upper levels are calculated for each optical transition using the Numerov method [32] with the respective potentials, and their difference “cal” is subtracted from the measured frequency “obs”. The parameters  $a_i$ ,  $\alpha_i$  and  $v_i$  are adjusted searching for a minimum of  $\chi^2$

$$\chi^2 = \sum_j \left( \frac{\text{obs}_j - \text{cal}_j}{\Delta \text{obs}_j} \right)^2, \quad (10)$$

$\Delta \text{obs}_j$  is the uncertainty of the experimental value. The fitting strategies for this nonlinear problem are provided by the MINUIT program package [33].

## 5 Results and discussion

Some frequency differences between  $^{127}\text{I}_2$  lines were also derived from the new recordings and included in the data set, and moreover, the recent absolute frequency measurements of the P(62) line of the (4–5) band at 661 nm by Badr et al. [34], of the P(80) (21–1) at 564 nm and the P(10) (14–1) at 585 nm by Reinhardt et al. [35] and of the P(42) (1–14) at 735 nm and R(114) (2–11) at 735 nm recently by Reinhardt et al. [36] were added to the data set. As for the near infrared range, also new frequencies of lines of high  $J''$  of the (0–15) band determined recently with a frequency comb in Amsterdam have been included. If the new literature data contained a sufficient number of hyperfine components, the hyperfine structure was fitted, and then the contribution of the hyperfine interaction was subtracted to yield the frequency of the rovibronic transition. In the other cases the hyperfine splitting was calculated taking the models from [12] and subtracted to yield the hyperfine-structure-free frequencies. The uncertainty introduced by this prediction of hyperfine splitting is less than 60 kHz [12].

Together with the data base from [7], now more than 1900 frequencies or frequency differences were available, of which about 290 are for the homonuclear isotopomer  $^{127}\text{I}_2$  and 90 are for the mixed species  $^{127}\text{I}^{129}\text{I}$ , for which a range of vibrational quantum numbers  $9 \leq v' \leq 21$  is covered in the upper state and  $0 \leq v'' \leq 5$  for the lower state.

In our previous paper BOC parameters were only taken into account for the excited B state. The BOC contributions to the low levels of the ground state involved here were expected to be small, because other states contributing to BOC are energetically far off and the energy interval of the observations in the X state is small.

In principle these arguments still apply to the present data set, but with the highly accurate data it is worthwhile to check whether BOC for the ground state can be determined now with some significance. Thus we ran a number of different fits on the same data set. Again, as in our previous paper [7], the minimum uncertainty of the absolute data was set to 3 MHz, in order to avoid placing too much weight on the most precise data. For the frequency differences gathered in the present work we chose an uncertainty of 2.1 MHz. A set of distinct fits was run:

1. with the same parameter set as before in [7]:  $a_0 - a_{31}$  and BOC parameters  $\alpha_0 - \alpha_4$  and  $v_0 - v_2$  for the B state,  $a_0$  to  $a_{13}$  and no BOC parameters for the X state;
2. case (1) parameters plus the leading nonadiabatic BOC parameter  $\alpha_0$  for the ground state;
3. case (1) plus the leading adiabatic BOC parameter  $v_0$  for the ground state;
4. case (1) plus BOC parameters  $\alpha_0$  and  $v_0$  for the ground state;
5. case (1) plus BOC parameters  $\alpha_5$  for the upper and  $v_0$  for the ground state;
6. case (1) plus two additional BOC parameters  $\alpha_5$  and  $v_3$  for the B state;
7. case (1) plus two additional high-order potential parameters  $a_{32}$  and  $a_{33}$  for the B state.

A fit to case (1) yields  $\chi^2 = 1128$  as a reference. Allowing for one or two additional BOC parameters,  $\chi^2$  of the fits was always reduced with respect to the first case. However, adding two potential parameters (case (7)), gave no significant decrease of  $\chi^2$ . This is not surprising, because the radial range is not increased with the new data of the present work as compared to [7]. However, this also shows that the improvement of  $\chi^2$  is not a result of adding two arbitrary parameters to the fit, and supports the importance of the resulting BOC functions from this evaluation. The smallest  $\chi^2$  was achieved with either the lowest order nonadiabatic BOC parameter  $\alpha_0$  for the ground state (case (2)), with two BOC parameters of lowest order for the ground state (case (4)), or with two additional BOC parameters for the upper state (case (6)). These results were practically of the same statistical significance, with a reduction of  $\chi^2$  by about 5% with respect to the first case above, corresponding to a dimensionless root-mean-square standard deviation  $\sigma = \sqrt{\frac{\chi^2}{N-M}} = 0.75$ . Here  $N$  is the total number of data and  $M$  the number of free parameters in the fit.

Inspection of the covariance matrix for the case of BOC parameters for the ground state reveals a correlation coefficient of 0.55 for the correlation of  $\alpha_0$  of the ground state with  $\alpha_0$  of the upper state. Also correlation coefficients larger than 0.1 for correlation with the other nonadiabatic

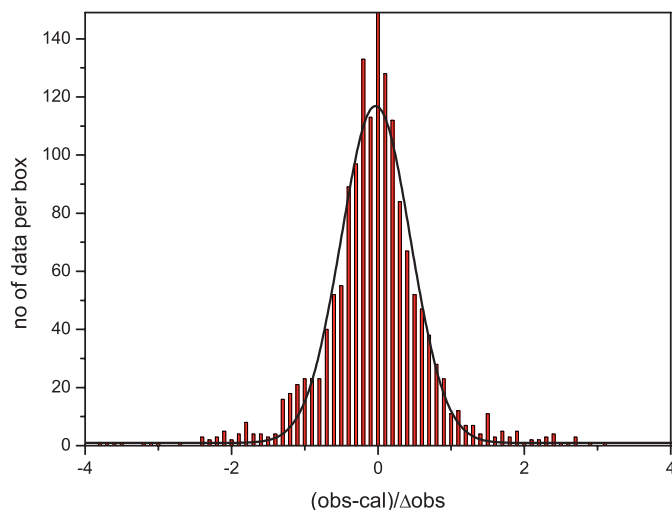


**Fig. 4.** (Color online) Histogram of the relative residuals of the fit. The curve represents a Gaussian distribution with a width of  $0.431(7)$  and position  $-0.029(7)$ .

BOC parameters of the upper state appear, while other correlations are less than 0.06. A similar correlation is observed for  $v_0$  of the ground state for correlations with the corresponding BOC parameters of the upper state. The parameter  $v_0$  represents the shift of the corresponding potential at  $R_m$  depending on the isotopomer. Hence one can already expect that only the differences can be determined, but not the individual well depths. The correlation between the BOC parameters of the upper and lower state confirms, that a physical distinction between the values of upper and lower state parameters is not reached yet, and is consistent with the observation, that the fit results for cases (2), (4), and (6) are essentially equivalent.

Consequently, we apparently cannot determine the significance of the BOC parameters for the ground state because of the correlation between lower and upper state BOC parameters. Thus we prefer to give as the final result the parameters from the fit of case (6), in which one additional parameter each for nonadiabatic and adiabatic BOC for the upper state was adjusted. The parameters for the potentials, the nonadiabatic and adiabatic Born-Oppenheimer corrections and all other parameters used in the fit are given in Table 1. At the end of the table the conventional parameters  $R_e$  and  $T_e$  for the resulting potentials are given for convenience.

The distribution of the relative fit residuals, being the residuum (obs - cal) divided by the experimental uncertainty of the datum, is shown by the histogram in Figure 4. A Gaussian function was fitted to the distribution and is displayed as the black curve. Its full width at half maximum (FWHM) is close to 1, which means that 66% of the residuals fall within an interval of  $\pm 0.5$  around the center. The center is slightly displaced by 0.029, corresponding to about 82 kHz for the data with highest precision, which means the minimum uncertainty of 3 MHz here. This shift is small and can be neglected for prediction of line frequencies from the parameters in Table 1. The new data on the

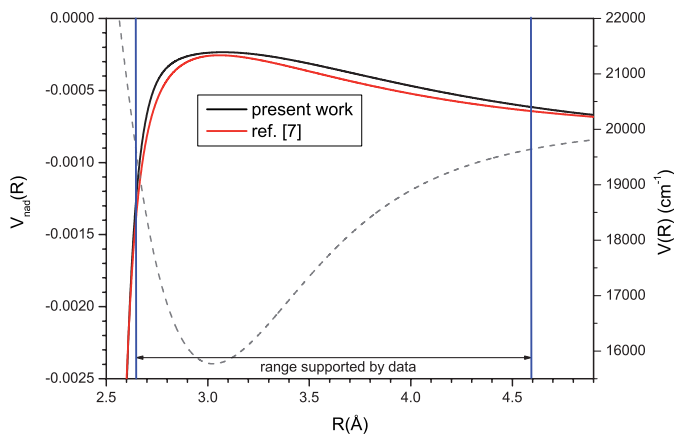


**Fig. 5.** (Color online) Comparison of the present nonadiabatic BOC function with that from [7]. The potential of the B state, given as the dashed line, has a similar position of the minimum as  $V_{nad}(R)$  for the maximum.

isotopomers  $^{129}\text{I}_2$  and  $^{127}\text{I}^{129}\text{I}$  are of similar precision compared to those of the main isotope and cover now a fairly broad range of vibrational quantum numbers in the upper and in the lower state. As discussed above, it turns out that two additional parameters for both the adiabatic and the nonadiabatic BOC functions improve the fit. The resulting BOC functions (nonadiabatic and adiabatic corrections) are displayed in Figures 5 and 6. We give for comparison also the functions reported in [7]. In the earlier work the results of the adiabatic correction were based only on 5 frequencies of the other isotopomers. The vertical (blue) lines mark the range of turning points of the vibrational motion of the nuclei, which is supported by the data. Within this range the nonadiabatic BOC function in Figure 5 has changed only slightly, its magnitude has decreased by about  $0.3 \times 10^{-4}$  compared to the old curve, and also the shape is nearly the same. The adiabatic contribution is close to the old function in the vicinity of the equilibrium internuclear distance, but it has smaller absolute values than the old one when going to the lower or upper data range limit. We emphasize that the functions are still effective functions, on the one hand, because we were not able to separate the contributions of the upper and the lower state due to the correlations between the BOC parameters and, on the other hand, because the nonadiabatic contribution from the kinetic energy operator is still absorbed in them.

To the best of our knowledge no other investigations of BOC function in iodine exist, and moreover, no theoretical estimations or ab initio calculations were found in the literature. So with these results we cannot go further by comparing them to theoretical results, or using theoretical results to obtain a distinction between upper state and lower state contributions.

## 6 Conclusion

We present new measurements of very precise rovibronic transition frequencies in the B-X system of the iso-

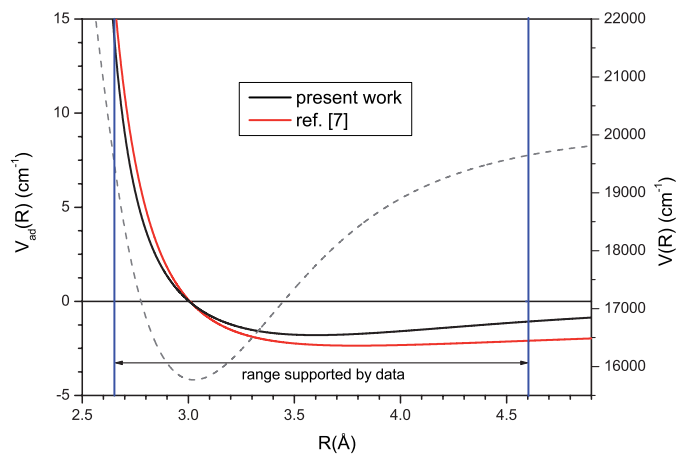


**Fig. 6.** (Color online) Comparison of the present adiabatic BOC function with that from [7]. To compare it with the total energy, the potential for the B state is given as dashed line.

topomers  $^{129}\text{I}_2$  and  $^{127}\text{I}^{129}\text{I}$  of the iodine molecule. The extended data set (now 380 lines, before 5) was used to derive model potentials and Born-Oppenheimer correction functions. The BOC functions are crucial for the accurate modeling of the spectrum, but in spite of the high accuracy of the present data set, the BOC contributions of the upper and the lower state cannot yet be separated due to correlations. The effective BOC contributions seem to be well determined. The difference energy  $T_e$  of the potential minima between B and X state, whose isotopic dependence is determined by the adiabatic BOC contribution, varies by  $T_e(^{127}\text{I}_2) - T_e(^{129}\text{I}_2) = 94(11)$  MHz, when comparing the potentials of  $^{127}\text{I}_2$  with those of  $^{129}\text{I}_2$ . This value was stable in the various fits described above to within the quoted  $1\sigma$  standard deviation.  $R_e$  is the same for  $^{129}\text{I}_2$  within the digits given in Table 1. Further interpretation is not yet possible due to the lack of theoretical calculations or modeling.

The derived model parameters can be used to calculate the rovibrational spectrum of all three isotopomers of the iodine molecules with a precision of about 1.5 MHz for a prediction to within a  $1\sigma$  uncertainty margin for the quantum number range of the observations. Perturbations were not observed in the spectral range covered by the data, thus we have good reason that the description for the isotopomers  $^{129}\text{I}_2$  and  $^{127}\text{I}^{129}\text{I}$  can be extrapolated from the whole range of quantum numbers for the main isotopomer.

Together with the recently published models of the hyperfine structure a model system is available now, which allows to predict iodine lines including the hyperfine structure with essentially the uncertainty stated above.

In several regions of the total range, where the iodine B-X spectrum can be observed, lines with less precise frequencies only are available yet. Here the prediction uncertainty is also reduced. For a more detailed picture of the spectral ranges and the corresponding prediction accuracy, the reader is referred to Figure 3 in our previous paper [7].

As a next step in this project, further precise measurements of iodine lines in the near infrared spectral region are planned, where the frequencies will be determined by use of a frequency comb based on a femtosecond pulsed laser.

This study is supported by the European Community, Integrated Infrastructure Initiative action (RII3-CT-2003-506350) and by the Netherlands Foundation for Fundamental Research of Matter (FOM).

## References

1. T.J. Quinn, *Metrologia* **40**, 103 (2003)
2. S. Gerstenkorn, P. Luc, *Atlas du spectre d'absorption de la molécule d'iode*, Laboratoire Aimé Cotton, CNRS II, Orsay (France), 14 000 cm<sup>-1</sup> – 15 600 cm<sup>-1</sup> (1978), 15 600 cm<sup>-1</sup> – 17 600 cm<sup>-1</sup> (1977), 17 500 cm<sup>-1</sup> – 20 000 cm<sup>-1</sup> (1977); S. Gerstenkorn, J. Vergès, J. Chevillard, *Atlas du spectre d'absorption de la molécule d'iode*, Laboratoire Aimé Cotton, CNRS II, Orsay (France), 11 000 cm<sup>-1</sup> – 14 000 cm<sup>-1</sup> (1982)
3. H. Katô, M. Baba, S. Kasahara, K. Ishikawa, M. Misono, Y. Kimura, J. O'Reilly, H. Kuwano, T. Shimamoto, T. Shinano, C. Fujiwara, M. Ikeuchi, N. Fujita, M.H. Kabir, M. Ushino, R. Takahashi, Y. Matsunobu, *Doppler-Free High Resolution Spectral Atlas of Iodine Molecule* (Japan Society for the Promotion of Science, 2000)
4. S.C. Xu, R. van Dierendonck, W. Hogervorst, W. Ubachs, *J. Mol. Spectrosc.* **201**, 256 (2000)
5. I. Velchev, R. van Dierendonck, W. Hogervorst, W. Ubachs, *J. Mol. Spectrosc.* **187**, 21 (1998)
6. C.J. Sansonetti, *J. Opt. Soc. Am. B* **14**, 1913 (1997)
7. H. Knöckel, B. Bodermann, E. Tiemann, *Eur. Phys. J. D* **28**, 199 (2004)
8. J.K.G. Watson, *J. Mol. Spectrosc.* **80**, 411 (1980)
9. S. Gerstenkorn, P. Luc, *J. Phys.* **46**, 867 (1985)
10. D. Cerny, R. Bacis, J. Vergès, *J. Mol. Spectrosc.* **116**, 458 (1986)
11. B. Bodermann, H. Knöckel, E. Tiemann, *Eur. Phys. J. D* **19**, 31 (2002)
12. E.J. Salumbides, K.S.E. Eikema, W. Ubachs, U. Hollenstein, H. Knöckel, E. Tiemann, *Molec. Phys.* **104**, 2641 (2006)
13. Landolt-Börnstein, *Funktionen und Zahlenwerte aus Physik, Chemie, Astronomie* (Springer, Berlin, 1960)
14. R.K. Raj, D. Bloch, J.J. Snyder, G. Camy, M. Ducloy, *Phys. Rev. Lett.* **44**, 1251 (1980)
15. J.J. Snyder, R.K. Raj, D. Bloch, M. Ducloy, *Opt. Lett.* **5**, 163 (1980)
16. L. Chen, W.-Y. Cheng, J. Ye, *J. Opt. Soc. Am. B* **21**, 820 (2004)
17. J.P. Pique, F. Hartmann, S. Churassy, R. Bacis, *J. Phys.* **47**, 1909 (1986)
18. J.P. Pique, F. Hartmann, S. Churassy, R. Bacis, *J. Phys.* **47**, 1917 (1986)
19. J. Vigué, M. Broyer, J.C. Lehmann, *J. Phys.* **42**, 937 (1981)
20. J. Vigué, M. Broyer, J.C. Lehmann, *J. Phys.* **42**, 949 (1981)
21. J. Vigué, M. Broyer, J.C. Lehmann, *J. Phys.* **42**, 961 (1981)
22. J.Y. Seto, Z. Morbi, F. Charron, S.K. Lee, P.F. Bernath, R.J. Le Roy, *J. Chem. Phys.* **110**, 11756 (1999)
23. J.Y. Seto, R.J. Le Roy, J. Vergès, C. Amiot, *J. Chem. Phys.* **113**, 3067 (2000)
24. R.J. Le Roy, Y. Huang, C. Jary, *J. Chem. Phys.* **125**, 164310 (2006)
25. A. Pashov, W. Jastrzebski, P. Kowalczyk, *Comput. Phys. Commun.* **128**, 622 (2000)
26. R. Bacis, D. Cerny, F. Martin, *J. Mol. Spectrosc.* **118**, 434 (1986)
27. S. Gerstenkorn, P. Luc, R.J. Le Roy, *Can. J. Phys.* **69**, 1299 (1991)
28. S. Gerstenkorn, P. Luc, C. Amiot, *J. Phys.* **46**, 355 (1985)
29. J.K.G. Watson, *J. Mol. Spectrosc.* **217**, 157 (2003)
30. M. Rey, V.G. Tyuterev, J.A. Coxon, R.J. LeRoy, *J. Mol. Spectrosc.* **238**, 260 (2006)
31. R.J. Le Roy, Y. Huang, *J. Mol. Struct. Theochem* **591**, 175 (2002)
32. J.M. Blatt, *J. Comput. Phys.* **1**, 382 (1967)
33. F. James, M. Roos, *D506 Minuit* (Cern library PACKLIB, 1989)
34. T. Badr, J.-P. Wallerand, P. Juncar, M.E. Himbert, D.J.E. Knight, M.D. Plimmer, Poster on the ETTF05, European Forum on Time and Frequency, Bescançon, France (2005)
35. S. Reinhardt, G. Saathoff, S. Karpuk, C. Novotny, G. Huber, M. Zimmermann, R. Holzwarth, T. Udem, T.W. Hänsch, G. Gwinner, *Opt. Commun.* **261**, 282 (2006)
36. S. Reinhardt, B. Bernhardt, C. Geppert, R. Holzwarth, G. Huber, S. Karpuk, N. Miski-Oglu, W. Nörtershäuser, C. Novotny, Th. Udem, *Opt. Commun.* **274**, 354 (2007)
37. Chun-Chieh Liao, Kuo-Yu Wu, Yu-Hung Lien, Jow-Tsong Shy, H. Knöckel, E. Tiemann, to be published